Macromolecular Materials and Engineering

Macromolecular Materials and Engineering Open Access
www.mame-journal.de

RESEARCH ARTICLE OPEN ACCESS

Colorimetric Detection of Nickel Ions Using Bacterial Nanocellulose Paper-Based Strips

Admilton A. P. Santana[1] | José Felipe dos Santos[1] | Jonatas De Oliveira S. Silva[1] | Kelcilene B. R. Teodoro[2] | Daniel S. Correa[2] | Rodolfo M. M. Santana[1] | Luiza A. Mercante[1]

[1]Institute of Chemistry, Federal University of Bahia (UFBA), Salvador, Bahia, Brazil | [2]Nanotechnology National Laboratory For Agriculture (LNNA), Embrapa Instrumentação, São Carlos, São Paulo, Brazil

Correspondence: Luiza A. Mercante (lmercante@ufba.br)

Received: 18 June 2025 | **Revised:** 28 August 2025 | **Accepted:** 15 September 2025

Funding: This study was supported by Conselho Nacional de Desenvolvimento Científico e Tecnológico (CNPq, grant number: 406925/2022-4) and Fundação de Amparo à Pesquisa do Estado de São Paulo (FAPESP, grant numbers: 2018/18468-2, 2023/13428-0).

Keywords: cellulose | digital image colorimetry | disposable sensors | paper-based analytical devices | sustainable materials

ABSTRACT

Bacterial nanocellulose (BNC) has proven to be an excellent platform for developing sustainable optical (bio)sensors due to its exceptional properties, including optical transparency, high porosity, and large surface area. These features enable uniform dye distribution, thereby mitigating issues commonly found in paper-based devices, such as low dye immobilization and non-uniform color response. Herein, we report a simple, affordable (~$0.03/strip) BNC-based colorimetric strip for detecting Ni^{2+} ions using digital image analysis. The strips were prepared by functionalizing BNC membranes with the dye 4-(2-thiazolylazo)resorcinol (TAR), a complexing agent widely used for the detection of metal ions. Physicochemical characterization confirmed the presence of a porous, interconnected nanofiber network and a hydroxyl-rich surface, which enabled effective and uniform dye incorporation. The BNC@TAR strips exhibited a linear response up to 10 mg L^{-1} and a limit of detection of 0.18 mg L^{-1}. The sensor fabrication process was highly reproducible, and the strips exhibited long-term stability, maintaining their analytical performance even after 40 days of storage. The strips were also applied to real water analysis, yielding recovery values ranging from 93.1% to 103.4%. These findings support the potential of BNC as a sustainable substrate for developing low-cost, disposable colorimetric sensors for on-site environmental monitoring.

1 | Introduction

Recent advances in sensing technology based on nanomaterials, driven by a growing market projected to reach $33 billion by 2030 [1], have led to increased interest in exploring novel substrates for developing miniaturized, flexible, and disposable sensing devices [2, 3]. In this regard, biopolymers such as chitin, lignin, and cellulose offer a promising avenue for advancing sensor technology due to their biodegradability, biocompatibility, abundance, and diverse functionality [4–8]. Among these, bacterial nanocellulose (BNC), which shares a similar component and structure with paper, is a particularly noteworthy bio-platform for fabricating paper-based sensors [9, 10]. Produced through the microbial fermentation of sugars and organic substrates by species such as *Komagataeibacter xylinum* and *Komagataeibacter hansenii* [11], BNC exhibits unique characteristics, including optical transparence, high porosity, a 3D fibrillar network, large specific surface area, thermal resistance, mechanical flexibility, and chemical stability [12, 13]. These features underscore its multifunctionality and enhance its capacity to immobilize active compounds through its porous nature and abundant hydroxyl groups [11, 14, 15]. Consequently, BNC membranes are considered

ideal materials for developing sustainable, disposable, and low-cost colorimetric sensors [12].

The effectiveness of BNC as a functional substrate for colorimetric paper-based sensors has been demonstrated in previous works. Moeinpour's group, for instance, showed that BNC is an ideal substrate for the uniform immobilization of anthocyanin, enabling the on-site detection of metal ions (Al^{3+}, Cu^{2+}, Hg^{2+}) in different matrices [15–18]. Similarly, Faham et al. [14] and Milindanuth et al. [19] demonstrated that BNC's porous and chemically stable architecture enables the efficient distribution of curcumin and rhodamine B, preserving their optical properties, which allows for the high-sensitivity colorimetric detection of Fe^{3+} and Cu^{2+} ions, respectively. These applications demonstrate the versatility of BNC for on-site colorimetric sensing, offering efficient analytical performance without the need for complex instrumentation. Despite these results, to the best of our knowledge, BNC membranes have not been applied as substrates for Ni^{2+} colorimetric monitoring. This is particularly relevant since Ni^{2+} is a significant environmental pollutant, and excessive exposure can lead to severe health issues, including dermatitis, lung cancer, and lung fibrosis [20].

In this context, we report the development of a simple, low-cost, and environmentally friendly colorimetric sensor strip for Ni^{2+} detection based on a BNC membrane functionalized with 4-(2-thiazolylazo)resorcinol (TAR), a chromogenic compound widely employed in metal ion analysis due to its strong complexation ability [21, 22]. The strips were then used in conjunction with digital image analysis, rather than conventional spectrophotometric measurement, enabling on-site detection. The system combines straightforward fabrication with high sensitivity, selectivity, and reproducibility, attributed to the synergistic effect between TAR functional groups and the unique physicochemical characteristics of BNC. Further attempts to analyze Ni^{2+} ions in real environmental water samples confirmed the potential of this sensor as a portable, sustainable, and accurate platform for visual monitoring of metal ions with high accuracy and reliability.

2 | Materials and Methods

2.1 | Reagents and Solutions

Bacterial nanocellulose (BNC) membranes were purchased from HB Biotech (Araraquara, Brazil). 4-(2-thiazolylazo)resorcinol (TAR), acetic acid, $Fe(NO_3)_3.9H_2O$, NaOH, $Cd(NO_3)_2.4H_2O$, $CoCl_2.6H_2O$, and $Cr(NO_3)_3.9H_2O$ were purchased from Sigma–Aldrich (St. Louis, United States). Ethanol (99%), orthophosphoric acid (85%), boric acid, $Ni(NO_3)_2{\cdot}6H_2O$, NaCl, and NaF were obtained from NEON (São Paulo, Brazil). Na_2CO_3 and $Cu(NO_3)_2.3H_2O$ were obtained from Synth (São Paulo, Brazil). Chloroform was purchased from Isofar (Duque de Caxias, Brazil). $Ca(NO_3)_2$ was purchased from Specsol (Jacareí, Brazil). Sodium thiosulfate was purchased from Anidrol (Diadema, Brazil).

A TAR solution (5% w/v) was obtained by dissolving the proper amount of dye in an ethanol/chloroform mixture (80/20, v/v). Britton–Robinson (B–R) buffer solutions (0.5 mol L^{-1}) had their pH adjusted between 2.0 and 8.0 using HCl (3 mol L^{-1}) or NaOH (3 mol L^{-1}) solutions. A Ni^{2+} stock solution (250 mg L^{-1}) was prepared by dissolving the $Ni(NO_3)_2.6H_2O$ in B–R buffer (pH = 4.0). All aqueous solutions were prepared using ultrapure water obtained from a Milli-Q system (Millipore, Bedford, MA, USA) with a specific resistivity of 18.2 MΩ cm.

2.2 | Functionalization of Bacterial Nanocellulose Membranes

The BNC membrane (40 × 40 mm) was functionalized by immersion in 4 mL of TAR solution in a Petri dish for 15 min. After drying, the functionalized membrane was submerged in ultrapure water for 15 min to remove the excess of TAR, and then it was left to dry at room temperature. Then, the functionalized membrane (BNC@TAR) was cut to obtain sensor strips measuring 5.0 × 7.5 mm.

2.3 | Physicochemical Characterization

The morphology of the BNC membrane was investigated using a field-emission gun scanning electron microscopy (FEG-SEM, JEOL-JSM 6701F). X-ray diffraction (XRD) patterns were obtained using CuKα radiation from 5° to 40° at 2° min^{-1}, 30 kV, and 30 mA in a Shimadzu XRD-6000 diffractometer. The Fourier transform infrared spectroscopy (FTIR) spectra were acquired in attenuated total reflection (ATR) mode on a Bruker Vertex 70 equipment, where 64 scans with a resolution of 2 cm^{-1} were collected between 700 and 1700 cm^{-1}. The membranes were also characterized with diffuse reflectance spectroscopy (DRS) using a Thermo Scientific Evolution One Plus spectrophotometer. UV–vis spectroscopy was performed using a Shimadzu model UV-1800 spectrophotometer with a quartz cuvette having an optical path length of 1 cm.

2.4 | Colorimetric Detection of Ni^{2+} Ions

The colorimetric assays were performed in Eppendorf tubes, where the BNC@TAR strips were submerged in 200 µL of the Ni^{2+} solution. After the reaction, the strips were left to rest on paper towels for 15 min to remove excess water, and then they were submitted for digital image analysis. The digital images of BNC@TAR-Ni strips were acquired using a digital microscope (Haiz, USB 1600X) attached to a cardboard box as previously described in our previous work [23]. To ensure the reproducibility of the results, all images were captured using the same brightness and focus settings, with the distance between the strips and the microscope maintained at 50 mm to minimize errors during image capture. The RGB and its component values (Red, Green, and Blue) were obtained with the ImageJ software (National Institutes of Health, Bethesda, MD, USA). The same square region of interest (ROI) of 25 × 25 pixels was selected and applied to each digital image. Through the values obtained, the absorbance was calculated using the expression: absorbance = $-\log(I/I_0)$, where I_0 corresponds to the channel intensity value of the unreacted strip and I to the intensity of the reacted strip.

Different pH conditions, ranging from 2.0 to 8.0, and reaction times, ranging from 5 to 30 min, were evaluated to assess the effects of pH and time on the analytical response. The calibration curve was obtained by relating the absorbance of the Red channel

to the Ni^{2+} concentration ranging from 0.5 to 10 mg L^{-1}. The limits of detection (LOD) and quantification (LOQ) were calculated through the following expressions: LOD = 3.3(S_b/b) and LOQ = 3(LOD), where S_b corresponds to the standard deviation between the calculated absorbance values of BNC@TAR strips (n = 10), and b is the slope of the analytical curve.

The precision of the method was assessed by evaluating the relative standard deviation (RSD) values obtained when applying BNC@TAR strips (n = 6) in the analysis at 3 different Ni^{2+} concentrations (1, 6, and 10 mg L^{-1}). For the reproducibility tests, the color change of strips (n = 4) of 4 different BNC@TAR membranes was evaluated, and RSD values were obtained. The selectivity assay was conducted in the presence of 6 mg L^{-1} Ni^{2+} and 600 mg L^{-1} of the interferents, except for Co^{2+} and Cu^{2+}, whose concentration was evaluated at 60 mg L^{-1}. Moreover, the long-term stability was assessed by examining the absorbance values of BNC@TAR strips (n = 3) over 40 days. All measurements were conducted under optimal experimental conditions.

2.5 | Real Water Samples

The tap and stream water samples were taken at the Federal University of Bahia, and a bottled water sample was purchased from the local market. The samples were filtered using a 0.20 μm diameter filter and diluted (1:1) in B–R buffer (pH = 4.0). To evaluate potential matrix effects on sensor performance, the stream water sample was analyzed both with and without filtration. Then, they were fortified with different concentrations of Ni^{2+} (2, 4, and 8 mg L^{-1}), and sodium thiosulfate (600 mg L^{-1}) was added as a masking agent to prevent interference from Cu^{2+} and Co^{2+} [24, 25].

3 | Results and Discussion

3.1 | Physicochemical Characterization

XRD analysis (Figure 1a) of the BNC revealed a well-defined typical crystallographic pattern of cellulose, with two intense and sharp peaks at 2θ = 14.5° and 22.7°, corresponding to the (101) and (200) planes of cellulose type I structure, respectively [26, 27]. The FEG-SEM image (Figure 1b) of the BNC reveals the morphology of a characteristic porous membrane composed of an overlapping network of fine cellulose nanofibers with a uniform size distribution [28]. After dye impregnation, the FEG-SEM image of BNC@TAR (Figure S1a) indicates the maintenance of the BNC structure, with no significant changes observed in the membrane morphology or porosity.

The FTIR spectra of BNC and BNC@TAR (Figure 1c) exhibit similar profiles, since BNC is the major material in both samples. Characteristic peaks of cellulose are observed at 1427 and 1315 cm^{-1} (C—H bonds), 1161 cm^{-1} (C—O—C), 1107 cm^{-1} (C—O), and 1053 cm^{-1} (C—O—H) [29, 30]. In the BNC@TAR spectrum, additional bands of the chromogenic agent are observed at 1634 cm^{-1}, corresponding to the C═N stretching of the thiazole group, and at 1591 cm^{-1} attributed to the N═N stretching of the azo group. The bands at 1477 and 1255 cm^{-1} are related to the C═C and C—O stretching vibrations of the resorcinol group, respectively, and the band at 776 cm^{-1} is assigned to the C—S stretching of the thiazole group [31, 32]. As shown, the FTIR spectra of BNC after TAR modification exhibited no significant shifts compared to the pristine membrane, providing strong evidence that the dye is primarily immobilized via physical adsorption.

The membranes were also characterized by UV–vis DRS analysis (Figure 1d). As expected, due to its colorless nature, the BNC membrane shows no absorption bands in the UV–vis region [33]. After the TAR impregnation, three bands in the UV–vis region are observed, confirming the effective incorporation of the dye onto the surface of the BNC membrane. The bands at 223 and 267 nm are attributed to the π-π^* transition of the C═N and N═N bonds of the thiazole and azo groups, respectively. The broader and more intense band with a λ_{max} at 387 nm is associated with the n-π^* transition of the N═N bond in the azo group [32, 34]. Additionally, UV–vis analysis of the TAR solution (Figure S2) revealed three bands with λ_{max} at 263nm, 412 nm (shoulder), and 443 nm, corresponding to intra-ligand π–π^* and n-π^* transitions, respectively, consistent with the features observed in the DRS spectrum [32, 34].

3.2 | BNC@TAR Reactivity and Sensing Performance for Ni^{2+} Detection

The performance of BNC@TAR strips for nickel detection was initially assessed by visual evaluation of the color change after immersion in a standard aqueous Ni^{2+} solution (200 μL, 6 mg L^{-1}). After 15 min, a visible and homogenous color change from yellow to brownish-gray was observed (Figure 2a), resulting from the complexation between Ni^{2+} ions and the TAR functional groups. The effectiveness of TAR immobilization was further evaluated by analyzing randomly selected ROIs (n = 12) of BNC@TAR (Figure S2), yielding an RSD value of < 1.3%. This demonstrates a high homogeneity in the distribution of the chromogenic agent on the sensor surface, which enhances both the reproducibility and the applicability of the proposed sensor.

The FTIR spectrum of the reacted strip (BNC@TAR-Ni) (Figure 1c) revealed that the characteristic bands related to the N═N, C—O and C—S groups of TAR became less intense or disappeared after the reaction with Ni^{2+} ions, suggesting that the interaction with nickel alters the energy density around atoms directly involved in the coordination, confirming the formation of the Ni–TAR complex. Similar behavior can be observed in the DRS spectrum (Figure 1d), where the bands corresponding to the C═N and N═N bonds overlap or are shifted to higher wavelengths, supporting the involvement of the nitrogen atoms from the thiazole and azo groups, as well as the oxygen atom from resorcinol, in the coordination reaction with the nickel ion [31, 32, 34]. Additionally, after the reaction, a new band attributed to the Ni-TAR complex is observed at λ_{max} = 606 nm, which is associated with the d-d transition of Ni^{2+} ions [32]. This band intensity increases and overlaps with the band assigned to the n-π^* transition, as the nickel ion concentration increases. This overlapping leads to the brownish-gray color observed for the membrane after the reaction (Figure 2a), due to the absorption of radiation at multiple wavelengths across a broad region of the UV–vis spectrum. For the complex formed in solution (Figure S3), a decrease in the intensity of the 263 nm band

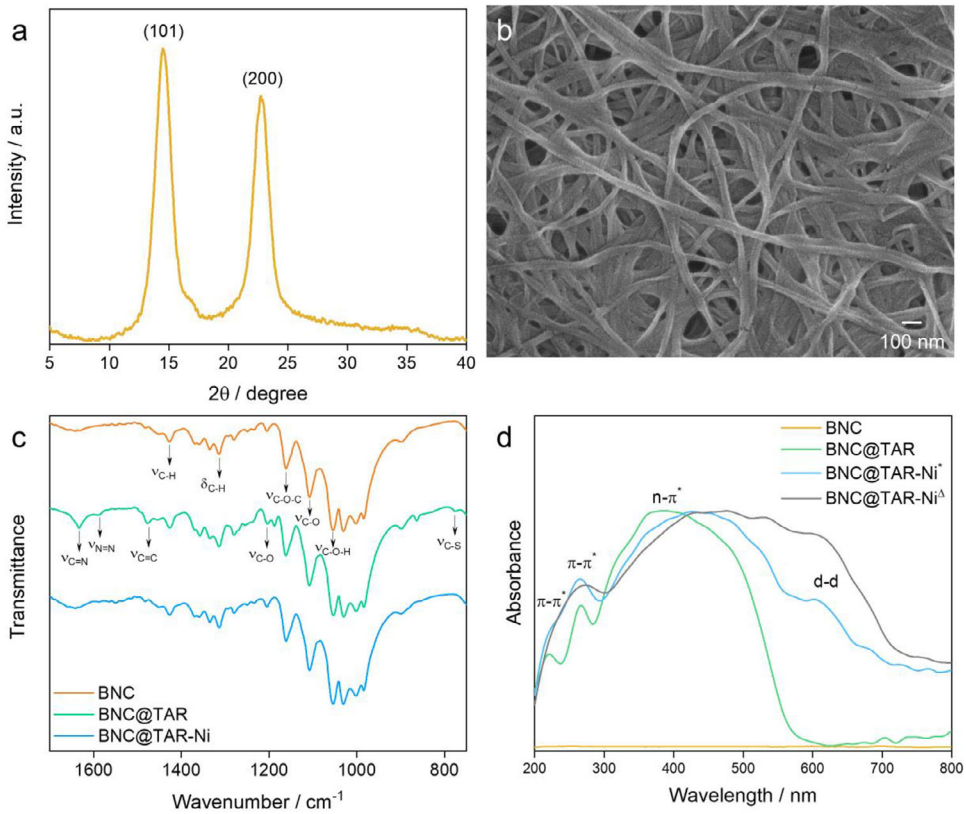

FIGURE 1 | (a) XRD pattern and (b) SEM image of BNC membrane. (c) FTIR and (d) diffuse reflectance spectra of BNC, BNC@TAR, and BNC@TAR-Ni membranes (* and Δ mean lower and higher concentration of nickel ions, respectively).

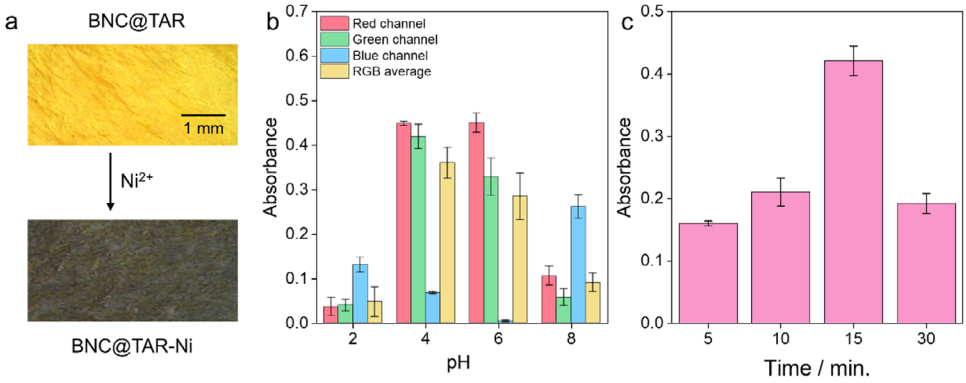

FIGURE 2 | (a) Digital images of the BNC@TAR strips before and after the reaction with Ni^{2+} ions (pH 4.0). (b) Variation of the absorbance values for RGB, Red, Green, and Blue channels (15 min) in the presence of 200 μL of Ni^{2+} solution (6 mg L^{-1}) under different pH conditions (B–R buffer, 0.5 mol L^{-1}). (c) Variation of the absorbance values for the Red channel in the presence of 200 μL of Ni^{2+} solution (6 mg L^{-1}) in B–R buffer (pH = 4.0) under different reaction times.

and the disappearance of the 412 nm shoulder were observed, while the band previously centered at 443 nm shifted slightly to 430 nm. In addition, two new bands at 551 and 583 nm, assigned to complex formation and the d-d transition of Ni^{2+}, respectively, were also observed. These findings indicate that the complexation mechanisms in solution and on the membrane are similar, occurring through a 2:1 TAR-to-Ni^{2+} stoichiometry.

The sensing performance of the BCN@TAR strips was further evaluated under different experimental conditions. Initially, the influence of pH (2.0, 4.0, 6.0, and 8.0) on the complexation reaction and color variation was evaluated by analyzing the absorbance values for RGB, and the individual Red, Green, and Blue channels (Figure 2b). At pH 2.0, only slight changes in channel intensities were observed, suggesting that at this pH value, H^+ and Ni^{2+} ions compete for the complexation sites of TAR [35, 36]. For pH levels of 4.0 and 6.0, more pronounced variations in the calculated absorbance values were observed, with the most significant changes occurring in the Red channel. As evidenced by the DRS analysis (Figure 1d), the absorption band attributed to complex formation appears in a spectral region between orange and red. Therefore, the intensity of the Red

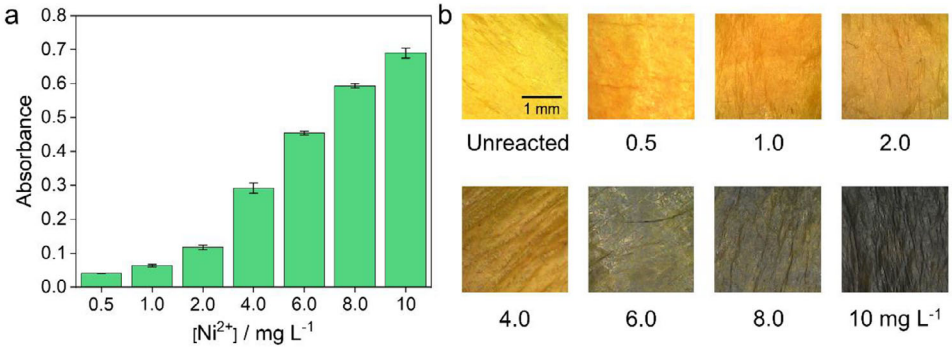

FIGURE 3 | (a) Variation of the absorbance values for the Red channel and (b) digital images of the BNC@TAR strips in the presence of different concentrations of Ni^{2+} under optimum conditions (15 min, pH 4.0).

channel varies due to the changes in the intensity of this band as more complexes are formed. Despite the similar behaviors, higher standard deviations were obtained for pH 6.0, indicating reduced reproducibility. At pH 8.0, leaching of the complex into the solution was observed (Figure S4), which compromised the colorimetric response. This behavior may be related to the deprotonation of TAR under these pH conditions, considering its pKa_1 value of 6.2 [37]. Once deprotonated, the negative charge is more effectively stabilized in the aqueous medium than on the BNC surface, potentially weakening its interaction with the membrane and contributing to signal instability. Based on these results, pH 4.0 and the Red channel were selected for further analysis.

The effect of immersion time of the BNC@TAR strips in the Ni^{2+} solution was also evaluated over a 5–30 min range (Figure 2c). The results showed a progressive increase in absorbance in the Red channel with immersion time, reaching a maximum at 15 min. For longer exposure times, a decrease in the absorbance value was observed, which may be attributed to the leaching of the complex from the membrane surface with increasing time (Figure S1b) [38, 39], resulting in a lower absorbance for periods longer than 15 min. Therefore, a reaction time of 15 min was selected for subsequent analyses, as it provided the highest signal intensity while reducing the analytical throughput.

Under optimized experimental conditions, the colorimetric response of the BNC@TAR strips was evaluated at varying Ni^{2+} concentrations (Figure 3a). Digital images of the membranes (Figure 3b) revealed a homogeneous color distribution over the BNC@TAR sensor strip for all tested concentrations, which positively impacts the sensor's reproducibility. A linear response ($R^2 = 0.996$) was obtained in the concentration range of 0.5–10 mg L^{-1} (Figure S5), and the LOD and LOQ values were calculated to be 0.18 and 0.55 mg L^{-1}, respectively.

The repeatability of the sensor was evaluated by comparing the absorbance values for 6 strips from the same membrane. The results showed a relative standard deviation (RSD) of 2.1%, corroborating the homogenous incorporation of the TAR across the membrane [12, 40]. To assess reproducibility, 4 strips from four independently prepared membranes were analyzed. An RSD of 3.7% was obtained, demonstrating high reproducibility in the functionalization process. Additionally, the storage stability experiments revealed that variations in absorbance values of less than 10% were observed over 40 days, indicating that the BNC@TAR strips exhibit excellent stability.

The analytical performance of the developed sensor was compared with previously reported colorimetric sensors for Ni^{2+} determination (Table S1). As shown, several paper-based colorimetric sensors have been reported for the detection of Ni^{2+}, differing mainly in the choice of substrate, chromogenic agent, detection range, and sensitivity. Most studies have relied on conventional filter papers, such as Whatman N°. 1, often combined with dimethylglyoxime (DMG) as the chromogenic reagent. These systems typically provide wide linear ranges, but their limits of detection (LOD) are usually relatively high, reaching values above 50 mg L^{-1} in certain reports. More sensitive configurations using the same DMG chemistry have been achieved, with LODs as low as 0.015 mg L^{-1}, although at the expense of a narrower linear range. Alternative approaches have employed different substrates, such as triacetylcellulose membranes or sol–gel-modified papers, and alternative chelating agents, including α-furyl dioxime and triazene derivatives, which have improved sensitivity but have not been widely explored. In this context, the present work introduces bacterial nanocellulose as a novel substrate coupled with TAR as the sensing reagent. Although not the lowest detection limit reported, the method offers a favorable balance between sensitivity and practical concentration range, while also ensuring reliable performance across diverse real water matrices, including tap, stream, and bottled water. Compared to conventional DMG-based systems, the BNC@TAR sensor offers a sustainable and innovative alternative, providing competitive analytical performance and broad environmental applicability. The BNC@TAR strips are also advantageous due to their low cost, estimated as US$0.03 per strip (Table S2).

The selectivity of the BNC@TAR strips toward potential interfering species was evaluated by analyzing variations in absorbance values in the presence of common inorganic ions typically found in environmental water samples (Na^+, Ca^{2+}, Fe^{3+}, Cd^{2+}, NO_3^-, F^-, Cr^{3+}, CO_3^{2-}, Co^{2+}, and Cu^{2+}). The results (Figure 4) showed no significant absorbance variations (<5%) for all tested ions except Co^{2+} and Cu^{2+}. The observed interferences from these ions are likely attributable to their strong affinity for the complexation sites of the TAR dye, leading to competitive binding with Ni^{2+} [31, 32, 34]. To prevent misinterpretation during sample analysis, sodium thiosulfate was successfully used as a masking agent for copper and cobalt ions [24, 25].

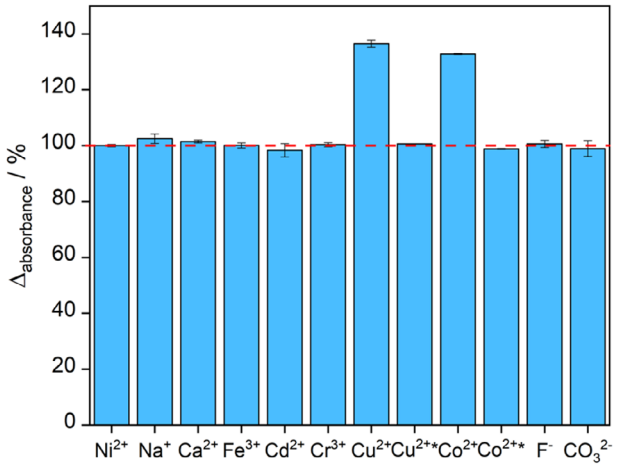

FIGURE 4 | Signal intensity variation for BNC@TAR strips in the presence of different concomitant species for the ratio 1:100 (Ni^{2+}:Concomitant) and 1:10 (Ni^{2+}:Cu^{2+} or Co^{2+}) under optimized analysis conditions. Cu^{2+}* and Co^{2+}* refer to the signal intensity variation caused by these ions in the presence of the masking agent.

TABLE 1 | Determination of Ni^{2+} in tap, stream, and bottled water samples using BNC@TAR strips (n = 3).

Samples	Added (mg L^{-1})	Measured (mg L^{-1})	Recovery (%)
Tap water	2.0	2.05 ± 0.01	102.86 ± 0.57
	4.0	4.10 ± 0.14	102.62 ± 3.53
	8.0	7.98 ± 0.21	99.78 ± 2.59
Filtered stream water	2.0	1.94 ± 0.07	97.20 ± 3.31
	4.0	3.72 ± 0.03	93.07 ± 0.83
	8.0	7.68 ± 0.03	96.10 ± 0.41
Unfiltered stream water	2.0	2.08 ± 0.03	96.07 ± 0.01
	4.0	3.86 ± 0.07	103.38 ± 0.02
	8.0	7.80 ± 0.12	102.47 ± 0.02
Bottled water	2.0	2.02 ± 0.04	100.85 ± 0.02
	4.0	3.92 ± 0.15	97.95 ± 0.04
	8.0	7.92 ± 0.15	98.99 ± 0.02

Subsequently, the robustness of the sensor strips was assessed through the analysis of real water samples, including tap water, stream water (both filtered and unfiltered), and bottled water, each spiked with three concentrations of Ni^{2+}. Recovery values (Table 1) ranging from 93.1% to 103.4% were obtained, confirming the suitability of the strips for routine environmental water analysis. Moreover, the recoveries obtained for the unfiltered stream water sample demonstrate that the potential matrix effects, such as turbidity or the presence of organic matter, do not significantly interfere with the sensor's analytical performance. The excellent sensor response across different water matrices reinforces the effectiveness of the BNC functionalized with TAR as an analytical tool and validates its applicability in real environmental contexts. Considering its sustainability, operational simplicity, and good analytical performance, the BNC@TAR sensor strips stand out as a practical, accessible, and reliable tool for on-site detection and monitoring of Ni^{2+} ions.

4 | Conclusion

Herein, a colorimetric sensor strip was successfully developed using bacterial nanocellulose membranes functionalized with TAR dye. The functionalization process follows a fast, simple, and cost-effective procedure, yielding efficient sensor strips (BNC@TAR) for the detection of Ni^{2+} ions within 15 min. Using digital image colorimetry, the strips exhibited a limit of detection of 0.18 mg L^{-1} and high selectivity against potential interfering species. The disposable sensor demonstrated remarkable repeatability, reproducibility, and long-term stability. Its practical applicability was confirmed through analyses of real water samples, including tap water, stream water, and bottled water. The outstanding analytical performance is primarily attributed to the intrinsic structural features of BNC, particularly its porous surface formed by an interconnected network of micro- and nanofibrils, which are rich in hydroxyl groups and promote the uniform distribution of the chromogenic agent, providing enhanced uniformity in the colorimetric response, as well as improved analytical stability and reproducibility. Overall, the BNC@TAR strips displayed reliable performance, reinforcing their potential for accessible and accurate colorimetric monitoring of Ni^{2+} contamination in diverse aqueous matrices. Furthermore, the limitations commonly associated with colorimetric paper-based sensors, such as a lack of standardization in image capture and the influence of ROI selection, were mitigated in our study through the use of a capture box with controlled lighting and the homogeneous color response of the BNC@TAR, ensuring reproducible measurements. Nevertheless, a comprehensive assessment of the sensor strips' life cycle and environmental impact will be necessary if commercialization is pursued.

Acknowledgements

The authors thank the financial support from Conselho Nacional de Desenvolvimento Científico e Tecnológico (CNPq, grant number: 406925/2022-4), Fundação de Amparo à Pesquisa do Estado de São Paulo (FAPESP, grant numbers: 2018/18468-2, 2023/13428-0), and Coordenação de Aperfeiçoamento de Pessoal de Nível Superior (CAPES—Brazil) – código de financiamento 001. AAPS thanks Fundação de Amparo à Pesquisa do Estado da Bahia for its scholarship.

Conflicts of Interest

The authors declare no conflicts of interest.

Data Availability Statement

The data that support the findings of this study are available from the corresponding author upon reasonable request.

References

1. A. Singh, E. Ahmed, M. D. Rather, et al., *Marketing Strategies in Nanomaterials for Sensor Applications: Bridging Lab to Market*, (Global Challenges, 2025).

2. A. Isa, M. Gharibi, A. Cetinkaya, and S. A. Ozkan, "Sustainable and Scalable Detection: Paper-Based Analytical Devices and Miniaturized Detection Systems for Modern Diagnostics," *Microchemical Journal* 212 (2025): 113210.

3. L. Kong, W. Li, T. Zhang, et al., "Wireless Technologies in Flexible and Wearable Sensing: from Materials Design, System Integration to Applications," *Advanced Materials* 36 (2024): 2400333.

4. V. Antanitta S, J. Patadiya, and B. Kandasubramanian, "Biopolymer-Chitin Products by Direct Ink Writing (DIW): a Review," *Hybrid Advances* 5 (2024): 100115.

5. A. N. Doyo, R. Kumar, and M. A. Barakat, "Recent Advances in Cellulose, Chitosan, and Alginate Based Biopolymeric Composites for Adsorption of Heavy Metals from Wastewater," *Journal of the Taiwan Institute of Chemical Engineers* 151 (2023): 105095.

6. K. Onofre-Rentería, D. A. Cabrera-Munguía, L. E. Cobos-Puc, J. A. Claudio-Rizo, L. Morales-Oyervides, and E. Oyervides-Muñoz, "Xanthan Gum Production and Its Modifications to Obtain Novel Applications: a Review," *Polymers for Advanced Technologies* 35 (2024): 70004.

7. N. A. A. Sezali, H. L. Ong, N. Jullok, A. R. Villagracia, and R. A. Doong, "A Review on Nanocellulose and Its Application in Supercapacitors," *Macromolecular Materials and Engineering* 306 (2021): 2100556.

8. A. Gebrekrstos, J. T. Orasugh, T. S. Muzata, and S. S. Ray, "Cellulose-Based Sustainable Composites: a Review of Systems for Applications in EMI Shielding and Sensors," *Macromolecular Materials and Engineering* 307 (2022): 2200185.

9. Y. Deng, S. Jiang, Z. Yan, Y. Chu, W. Wu, and H. Xiao, "Fluorescent Eu-MOF@Nanocellulose-Based Nanopaper for Rapid and Sensitive Detection of Uranium (VI)," *Analytica Chimica Acta* 1292 (2024): 342211.

10. S. Gomez-Gijon, I. Ortiz-Gómez, and A. Rivadeneyra, "Paper-Based Electronics: toward Sustainable Electronics," *Advanced Sustainable Systems* 9 (2024): 2400486.

11. H. Golmohammadi, E. Morales-Narváez, T. Naghdi, and A. Merkoçi, "Nanocellulose in Sensing and Biosensing," *Chemistry of Materials* 29 (2017): 5426–5446.

12. A. Suleimenova, M. F. Frasco, F. A. G. Soares da Silva, M. Gama, E. Fortunato, and M. G. F. Sales, "Bacterial Nanocellulose Membrane as Novel Substrate for Biomimetic Structural Color Materials: Application to Lysozyme Sensing," *Biosensors and Bioelectronics: X* 13 (2023): 100310.

13. F. Zhang, R. Shen, N. Li, X. Yang, and D. Lin, "Nanocellulose: an Amazing Nanomaterial with Diverse Applications in Food Science," *Carbohydrate Polymers* 304 (2023): 120497.

14. S. Faham, H. Golmohammadi, R. Ghavami, and G. Khayatian, "A Nanocellulose-Based Colorimetric Assay Kit for Smartphone Sensing of Iron and Iron-Chelating Deferoxamine Drug in Biofluids," *Analytica Chimica Acta* 1087 (2019): 104–112.

15. P. Parizadeh, F. Moeinpour, and F. S. Mohseni-Shahri, "Anthocyanin-induced Color Changes in Bacterial Cellulose Nanofibers for the Accurate and Selective Detection of Cu(II) in Water Samples," *Chemosphere* 326 (2023): 138459.

16. S. Arghavani, F. S. Mohseni-Shahri, and F. Moeinpour, "Anthocyanin-Loaded Bacterial Cellulose Nanofiber as a Green Sensor for Monitoring the Selective Naked Eye and Visual Detection of Al(III) Ions," *Analytical Science Advances* 4 (2023): 324–334.

17. M. Minabi-Nezhad, F. Moeinpour, and F. S. Mohseni-Shahri, "Development of a Green Metallochromic Indicator for Selective and Visual Detection of Copper(II) Ions," *Scientific Reports* 13 (2023): 12501.

18. M. Minabi-Nezhad, F. Moeinpour, and F. S. Mohseni-Shahri, "Anthocyanin-Enhanced Bacterial Cellulose Nanofibers for Sustainable Hg(II) Ion Sensing," *Starch/Staerke* 77 (2024): 2400064.

19. P. Milindanuth and P. Pisitsak, "A Novel Colorimetric Sensor Based on Rhodamine-B Derivative and Bacterial Cellulose for the Detection of Cu(II) Ions in Water," *Materials Chemistry and Physics* 216 (2018): 325–331.

20. S. Chakraborty and S. Rayalu, "Detection of Nickel by Chemo and Fluoro Sensing Technologies," *Spectrochimica Acta Part A: Molecular and Biomolecular Spectroscopy* 245 (2021): 118915.

21. F. I. El-Dossoki and F. A. El-Seify, "Physicochemical Studies on 4-(4′-Phenyl-2′-Thiazolylazo) Resorcinol and Its Complexation With Some Metal Ions," *Journal of Chemical & Engineering Data* 55 (2010): 3572–3577.

22. M. Wang, J. M. Lin, F. Qu, X. Shan, and Z. Chen, "On-capillary Complexation of Metal Ions with 4-(2-thiazolylazo)resorcinol in Capillary Electrophoresis," *Journal of Chromatography A* 1029 (2004): 249–254.

23. J. D. O. S. Silva, A. V. L. Capistrano, K. B. R. Teodoro, D. S. Correa, R. M. M. Santana, and L. A. Mercante, "Microfibrillated Cellulose-Based Colorimetric Sensor Strips for Detecting Total Iron in Water," *International Journal of Biological Macromolecules* 299 (2025): 140139.

24. A. J. Fischmann, A. C. Warden, J. Black, and L. Spiccia, "Synthesis, Characterization, and Structures of Copper(II)−Thiosulfate Complexes Incorporating Tripodal Tetraamine Ligands," *Inorganic Chemistry* 43 (2004): 6568–6578.

25. I. Povar, S. Ubaldini, T. Lupascu, O. Spinu, and B. Pintilie, "The Solution Chemistry Of The Copper (Ii)—Ammonia Thiosulfate Aqueous System, In: Simi," *National Research and Development Institute for Industrial Ecology* 21 (2018): 161–169.

26. T. Rattanawongwiboon, N. Khongbunya, K. Namvijit, et al., "Eco-Friendly Dye Adsorbent from Poly(vinyl amine) Grafted Onto Bacterial Cellulose Sheet by Using Gamma Radiation-Induced Simultaneous Grafting and Base Hydrolysis," *Journal of Polymers and the Environment* 32 (2024): 3048–3060.

27. K. Kupnik, M. Primožič, V. Kokol, Ž. Knez, and M. Leitgeb, "Antibacterial Komagataeibacter Hansenii Nanocellulose Membranes With Avocado Seed Bioactive Compounds," *Cellulose* 31 (2024): 4305–4327.

28. R. B. Sousa, A. C. Dametto, G. F. de Mesquita, et al., "Investigation of Bacterial Nanocellulose/Calcium Phosphates-based Composite Containing Cerium for Bone Repair," *Colloids and Surfaces B: Biointerfaces* 248 (2025): 114476.

29. T. Kondo, P. Rytczak, and S. Bielecki, *Bacterial nanocellulose*, (Elsevier, 2016), 59–71.

30. P. Sharma, M. Mittal, R. Sharma, A. Yadav, and N. K. Aggarwal, "Development of Bacterial Cellulose-based Nanocomposites Incorporated with Lignin and MgO as a Novel Antimicrobial Wound-dressing Material," *Iranian Polymer Journal* (2025).

31. A. Singh, C. L. Gehlot, and D. K. Singh, "Synthesis, Characterization, and Applications of a New Chelating Resin Containing 4-2-(Thiazolylazo) Resorcinol (TAR)," *Separation Science and Technology (Philadelphia)* 47 (2012): 2399–2407.

32. F. Karipcin, B. Dede, S. Percin-Ozkorucuklu, and E. Kabalcilar, "Mn(II), Co(II) and Ni(II) Complexes of 4-(2-Thiazolylazo)Resorcinol: Syntheses, Characterization, Catalase-Like Activity, Thermal and Electrochemical Behaviour," *Dyes and Pigments* 84 (2010): 14–18.

33. S. Liu, H. Lou, J. Luo, D. Albashir, Y. Shi, and Q. Chen, "A Novel in Situ Biosynthesized Bacterial Cellulose/MoS2/TiO2 Composite Film for Efficient Removal of Dyes and Pathogenic Bacteria from Industrial Wastewater under Sunlight Illumination," *ACS Appl Mater Interfaces* 17 (2025): 19543–19561.

34. F. Karipcin, E. Kabalcilar, S. Ilican, Y. Caglar, and M. Caglar, "Synthesized Some 4-(2-Thiazolylazo)Resorcinol Complexes: Characterization, Thermal and Optical Properties," *Spectrochimica Acta Part A: Molecular and Biomolecular Spectroscopy* 73 (2009): 174–180.

35. S. C. Low, N. A. binti Azmi, C. S. Ong, and J. K. Lim, "Environmental Monitoring of Trace Metal Pollutants Using Cellulosic-Paper Incorporating Color Change of Azo-Chromophore," *Environmental Science and Pollution Research* 29 (2022): 71614–71631.

36. A. Jo, G. Jang, H. Namgung, et al., "Simultaneous Detection and Removal of Radioisotopes with Modified Alginate Beads Containing

an Azo-Based Probe Using RGB Coordinates," *Journal of Hazardous Materials* 300 (2015): 227–234.

37. A. Benvidi, F. Heidari, R. Tabaraki, and M. Mazloum-Ardakani, "Application of Principal Component–Wavelet Neural Network in Spectrophotometric Determination of Acidity Constants of 4-(2-Thiazolylazo)-Resorcinol," *Spectrochimica Acta Part A: Molecular and Biomolecular Spectroscopy* 78 (2011): 1380–1385.

38. Y. M. Badiei, C. Traba, R. Rosales, et al., "Plasma-Initiated Graft Polymerization of Acrylic Acid Onto Fluorine-Doped Tin Oxide as a Platform for Immobilization of Water-Oxidation Catalysts," *ACS Applied Materials & Interfaces* 13 (2021): 14077–14090.

39. N. Ruecha, N. Soatthiyanon, C. Aumnate, Y. Boonyongmaneerat, and N. Rodthongkum, "Kenaf Cellulose-Based 3D Printed Device: a Novel Colorimetric Sensor for Ni(II)," *Cellulose* 27 (2020): 5211–5222.

40. M. Yang, D. Chen, J. Hu, X. Zheng, Z.-J. Lin, and H. Zhu, "The Application of Coffee-Ring Effect in Analytical Chemistry," *TrAC Trends in Analytical Chemistry* 157 (2022): 116752.

Supporting Information

Additional supporting information can be found online in the Supporting Information section.

Supporting File: mame70102-sup-0001-SuppMat.docx.